

## Feasibility of Vertical Rainwater Harvesting via In-situ Measurement of Wind-driven Rain Loads on Building Facades in a Tropical Climate

**Mozhgan Samzadeh**

Faculty of Built Environment, University of Malaya, 50603, Kuala Lumpur, Malaysia

**Nazli Che Din, Zunaibi Abdullah, Muhammad Azzam Ismail**

Department of Architecture, Faculty of Built Environment, University of Malaya, 50603, Kuala Lumpur, Malaysia

**Norhayati Mahyuddin**

Department of Building Surveying, Faculty of Built Environment, University of Malaya, 50603, Kuala Lumpur, Malaysia

### ABSTRACT

Rainwater is an alternative water resource to fulfill sustainable management of freshwater particularly in the regions receive abundant annual amounts of precipitation such as tropical Malaysia. To collect and store rainwater, rainwater harvesting system has been practiced since ancient from horizontal surfaces mostly rooftop of buildings in urban areas. Nowadays, this method in modern urban areas with tall buildings is considered inadequate and uneconomical because the ratio of facade surface areas is much higher than the ratio of roof surface areas. On the other hand, all rain has a horizontal velocity due to wind acting upon rain droplets which is called wind-driven rain (WDR). Growing tall buildings and the presence of WDR phenomenon make building façade surfaces the available promising surfaces to harvest substantial rainwater vertically and more efficiently. This article presents a one-year field measurement results that aims at quantifying the WDR loads impinged on the vertical facade areas of a pilot building located at the main campus of the University Malaya in Kuala Lumpur, Malaysia. Detailed descriptions of the gauge design, building, the measurements of on-site WDR, rainfall duration time, and weather data are presented. Records show that monsoon winds characteristics have significant influence on the WDR loads on the building facades compare to horizontal rainfall intensity. Finally, the collected in-situ data are exploited to validate data and determine WDR coefficient ( $\gamma$ ) to estimate the amount of WDR on a building façade via an empirical WDR relationship. Results show the feasibility of each square meter of vertical façade area to supply 12% of non-potable or 4.9% of potable water-usage per capita per day.

### Article History

Received: 05 January 2021

Received in revised form: 26 March 2021

Accepted: 17 May 2021

Published Online: 31 August 2021

### Keywords:

Wind-driven rain; Vertical Rainwater harvesting; Building facade; Measurement data; Monsoon wind

### Corresponding Author Contact:

nazlichedin@um.edu.my

DOI: 10.11113/ijbes.v8.n3.736

© 2021 Penerbit UTM Press. All rights reserved

### 1. Introduction

By 2030, the world is projected to face a 40% global water deficit under the business-as-usual (BaU) season (Connor, 2015), and the demand is expected to continue increasing at 1% per year until 2050, accounting for an increase of 20 to 30% above the current level of water use; mainly due to rising demand in the industrial and domestic sectors (WWAP, 2019). Over 2 billion people live in countries experiencing high water stress, and about 4 billion people experience severe water scarcity during at least one month of the year (WWAP, 2019).

The distribution and availability of freshwater resources, through precipitation and runoff, can be erratic, with different areas of the globe receiving different quantities of water over any given year (Connor, 2015).

In respect of the physical alternatives to fulfill sustainable management of freshwater, two main categories of solutions can be identified: (i) reduction of water consumption; and (ii) identification of new water resources (Silva et al., 2015). To date, much attention has been given to the former option and only limited attention has been given to the latter (Wu et al., 2017).

For buildings in general and residential buildings in particular, one of the most promising alternative water resources is the rainwater (Lade et al., 2015). Traditionally, the majority of researches have concentrated their studies on roof rainwater harvesting (RWH) system (Canavan, 2008; Cho et al., 2020; Dobravalskis et al., 2018). However, in urban areas with new tall buildings, the ratio of facade surface areas is much higher than the ratio of roof surface areas. Thus, rain more and mainly falls onto the buildings' facades and usually, rooftop rainwater collection can be considered inadequate (Adriano et al., 2011) or impossible when the roof has been used as a roof garden (SDI, 2003). On the other hand, as Dobravalskis et al. (2018) declared, all rain has a horizontal velocity due to wind acting upon rain droplets which is called wind-driven rain (WDR). Due to this characteristic, WDR hits all buildings' facades even those with a completely vertical angle, and it makes buildings' facades as the available potential surfaces for vertical RWH. This new approach to water resource management brings along more benefits in comparison with the horizontal RWH such as; harvesting potential cleaner water because it collects rainwater before ground/roof contamination occurs and utilizes without significant treatment for non-potable purposes; facade areas have not only larger surfaces but also are more unused spaces compared to rooftops in modern urban areas (Dobravalskis et al., 2018). Accordingly, new buildings can benefit from integrated vertical RWH from facade areas in order to optimize their water consumption and minimize their impact on the environment (Beorkrem et al., 2018). Wind-driven rain has been studied in building science as a moisture source with potential negative effects on the building envelope. But in a recent lab and miniature building ( $L \times W \times H = 1 \times 1 \times 2$  m<sup>3</sup>) experiment study by Cho et al. (2020), it has been declared that the amount of rainwater collected from the wall could be very significant compared to the roof area however, the amount of rainwater possibly obtained by a building facade has not been investigated yet. Their study recorded a total set of 40 WDR data collection with 1hr measurement duration for each in one year.

In this study, WDR as a potential water resource to be collected and utilized from vertical façade of buildings for rainwater harvesting system has been investigated. This real-time one-year wind-driven rain measurement method has been implemented for the first time to quantify the amount of accumulated rainwater impinging on a one-story building ( $L \times W \times H = 18.60 \times 6.40 \times 3.50$  m<sup>3</sup>) facades in a tropical climate as an alternative water resource for the rainwater harvesting system. According to the annual rainfall trends in Kuala Lumpur by UNFCCC (2015), rain mostly occurs in the afternoons and evenings, therefore only nocturnal precipitation (12 a.m. to 6 a.m.) was excluded in this study and a total set of 94 WDR data collection (~119 hrs.) events during one year were continuously recorded.

In terms of gauges neither standard design principles, nor industrial manufacturing exists to collect rainwater, and to the knowledge of the authors, so far no yearly measurement of WDR in building science has been applied in a tropical climate. This paper is divided into two parts (i) a brief review on the WDR gauge design principles, and (ii) results of a one-year experimental method to collect WDR from the vertical building facades at the campus of the University of Malaya in Malaysia. First part overviews design instructions and characteristics of seven different types of wall-mounted WDR gauges produced for the measurement purposes by researchers around the world in order to produce an accurate and reliable gauge for their measurement purposes. Second part presents the building, the gauge design instruction, and one-year experimental data collection and results.

### 1.1 Wind Driven Rain Definition

According to Foroushani (2013), WDR or driving rain is rain that is carried (driven) by wind and driven onto building envelopes with vector intensity causing oblique rain with the influence of gravity (Figure 1). Wind-driven rain or driving rain is the result of complex interactions among wind, rain, and building envelopes.

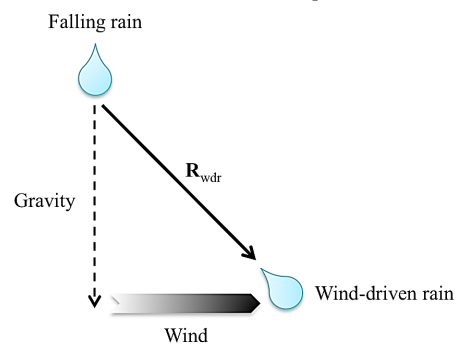


Figure 1 Wind-driven rain vector

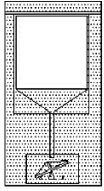
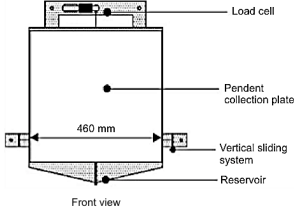
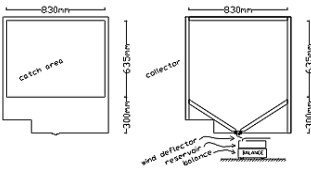
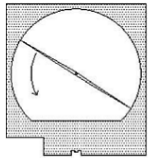
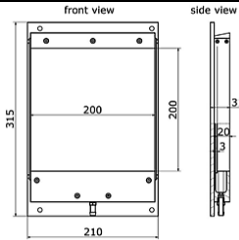
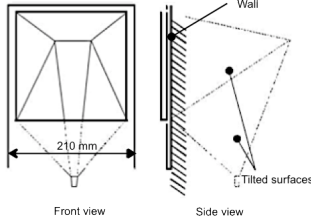
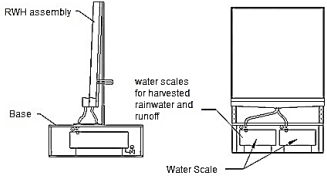
### 1.2 Wind Driven Rain Gauges

WDR gauges were initially made up of plate, composed of a collection area and a reservoir that are linked via a drainage channel Hogberg (1999); (Masters et al., 2013):

1. A catchment area (a shallow tray) mounted on the building facade; raindrops hit the tray, drip downwards and are collected via:
2. A drainage channel; which leads the collected rainwater to:
3. A reservoir or a water flux gauge; which enables the measurement of instantaneous driving rain intensities.

Seven different types of WDR gauges are presented in the following section. Table 1 illustrates the types of gauges, materials, sizes, and their function to wind-driven rain intensity.

**Table 1** Details of the applied WDR gauges

Name	Type	Principle	Material / Min. intensity	Catchment area
CTH		Traditional collector with tipping bucket ( $V_{tip}=1g$ )	Perspex (solid transparent plastic made of polymethyl methacrylate) $\frac{1g}{20min} = 0.09mm/h$	$0.18 \times 0.18 = 0.032 m^2$
TUD		Collector weighted by a strain gauge ( $\Delta m \approx 3g$ )	Stainless steel $\frac{1.3g}{10min} \approx 0.04 mm/h$	$0.46 \times 0.46 = 0.21 m^2$
TUE-I		Rectangular catchment area with reservoir (2 liters) and balance ( $\Delta m=1g$ )	Teflon coating (Polytetrafluoro ethylene) $\frac{0.1g}{20min} = 0.001mm/h$	$0.527 m^2$
TUE-II		Round catchment area with a rotating wiper with reservoir (3 liters) and balance ( $\Delta m=1g$ )	Teflon coating (Polytetrafluoro ethylene) $\frac{0.1g}{20min} = 0.001mm/h$	$0.492 m^2$
EMPA		Rectangular catchment area with reservoir (1 ml)	Aluminum & Glass $0.025 mm/h$ (10min period)	$0.2 \times 0.2 = 0.04 m^2$
TILTED-CTH-II		Collection area is tilted surfaces and deeply recessed	-	-
KUT		Square catchment area with two water-measuring scales for WDR and Rainwater Runoff	Stainless steel expanded metal mesh facade panel $0.14 mm/s \approx 0.005 mm/h$	$1 m^2$

1.2.1 CTH Gauge

The traditional WDR gauge (CTH) with a small catchment area was developed at the Chalmers University of Technology, Sweden. Its material is Perspex and the reservoir is measured by a tipping bucket with a tipping volume equal to 1g of water (Figure 2). “One tipping in 20 min represents a driving rain intensity of 0.09 mm/h” (Hogberg, 1998; Hogberg et al., 1999).

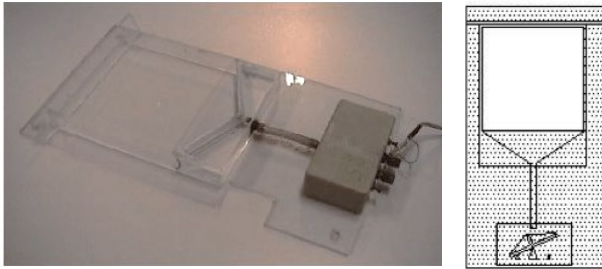


Figure 2 Wind-driven rain gauge CTH (from Hogberg et al. (1999))

1.2.2 TUD Gauge

Kragh et al. (1998) designed an improved WDR gauge at the Technical University of Denmark (TUD to reduce the measurement errors of remaining droplets on the catchment area (Figure 3). This gauge came with a ‘load cell’ on top of the device to record rainwater both in the reservoir and on the catchment area (Blocken et al., 2004). The collector is made out of a “stainless steel tray with a net mounted on the tray to reduce raindrop bouncing” (Hogberg et al., 1999). The Readings were recorded every 10 min to reduce the measurement error due to the sensitivity of the gauge to wind fluctuations (FJR van Mook, 2002).

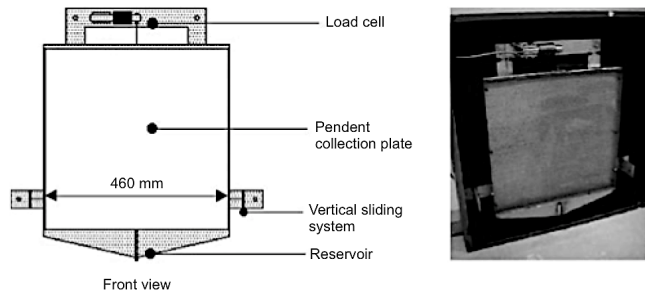


Figure 3 Wind-driven rain gauge TUD (FJR van Mook, 2002) from Blocken et al. (2006a) reused with permission)

1.2.3 TUE-I Gauge

The gauge TUE-I has been manufactured at the Eindhoven University of Technology, Netherlands. This gauge (Figure 4) has a larger catchment area (0.527 m<sup>2</sup>) compared to CTH (0.032 m<sup>2</sup>). Teflon surface finish intends to enhance the process of

dripping down the rainwater droplets to the reservoir (Hogberg et al., 1999). The drops collect by a large funnel to the reservoir (Van Mook, 1998). A balance measures the reservoir with an accuracy of 0.1g.

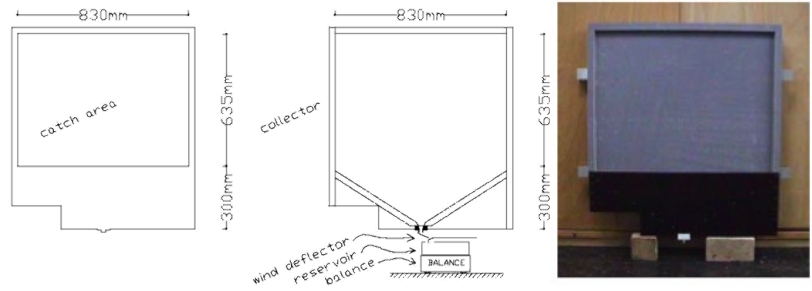
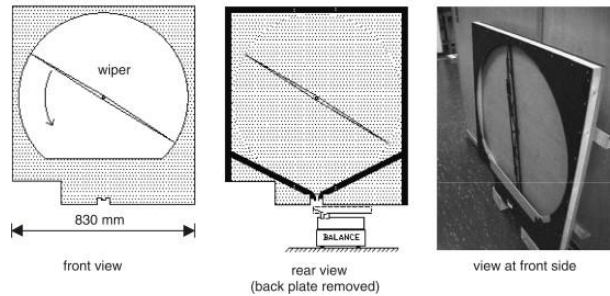


Figure 4 Wind-driven rain gauge TUE-I (from Van Mook (1998))

### 1.2.4 TUE-II Gauge

Gauge TUE-II is similar to gauge TUE-I, but it is equipped with a rotating wiper (Figure 5). The wiper collects all droplets on the catchment surface and doesn't let any remain on the surface. A

rain indicator automatically switches on the wiper. "The speed is approx. 1 rotation per 3 seconds; after every 5 seconds, the wiper rests during 5 s to reduce wear and tear" (Van Mook, 1998).



**Figure 5** Wind-driven rain gauge TUE-II from Blocken et al. (2006a) reused with permission)

### 1.2.5 EMPA Gauge

The EMPA WDR gauge was produced at the campus of the Swiss Federal Laboratories for Materials Science and Technology based on the guidelines of Blocken et al. (2006a) and Kubilay et al. (2014). The gauge frame is made of aluminum and the catch

surface is ordinary glass sheets to promote runoff (Figure 6). A connecting pipe conveys rainwater from catchment to the reservoir. The reservoir is placed inside the building to prevent frost and evaporation issues from the reservoir (Kubilay et al., 2014).

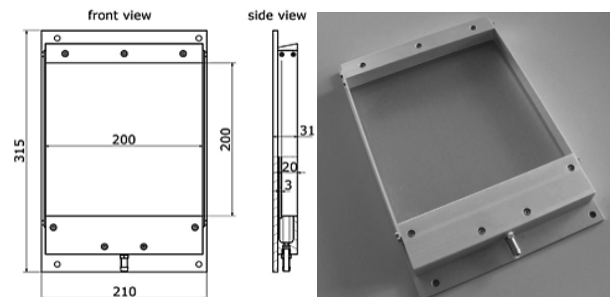


**Figure 6** Wind-driven rain gauge EMPA (from (Kubilay et al., 2014) reused with permission)

### 1.2.6 TILTED/CTH-II Gauge

Hogberg (2002) at the Chalmers University of Technology, Sweden developed a WDR gauge with a deeply recessed catchment area composed of tilted surfaces to prevent raindrops

splashing (Figure 7). In the Blocken et al. (2006a) was stated that the performance of this gauge in terms of the amount of accumulated rainwater was better than that of non-recessed gauges for high wind speed and heavy rainfall intensities.

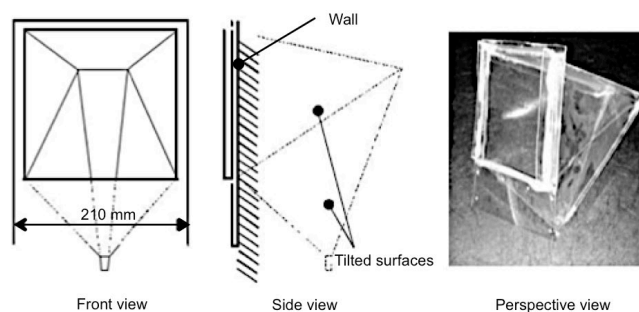


**Figure 7** Wind-driven rain gauge Tilted; CTH-II (© Hogberg (2002) from Blocken et al. (2006a) reused with permission)

### 1.2.7 KUT Gauge

The KUT gauge (Figure 8) was constructed in the Kaunas University of Technology, Lithuania to measure the rainwater collection rate (Dobravalskis et al., 2018). It is composed of two main parts; the RWH stand and the main control unit. The stand is a hermetic box with a depth of 58 mm: the front layer is an architectural facade panel of stainless steel expanded metal mesh.

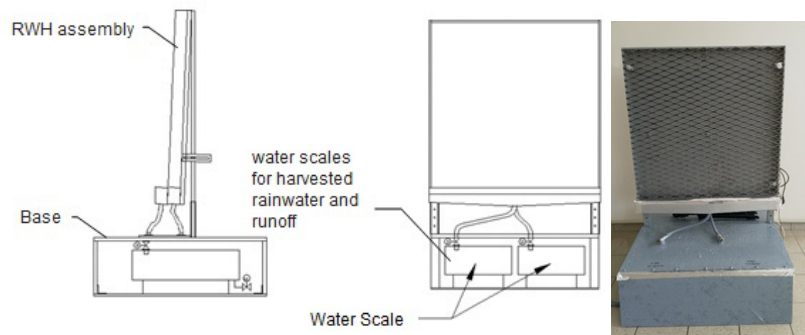


**Figure 8** Wind-driven rain gauge KUT (© Dobravalskis et al. (2018))

## 2. Material and Methods

### 2.1 Measurement Setup

The measurement setup is located at the main campus of the University of Malaya in the city of Kuala Lumpur, Malaysia, latitude  $3^{\circ}07'15''$  and longitude  $101^{\circ}39'23''$ . A pilot building was instrumented with 8 wind-driven rain gauges with high WDR acquisition resolution. The principal aim of this field measurement is to measure and compare the spatial distribution of WDR amount on the facades of the test building over a year from April 2017 to March 2018.

### 2.2 Climate

Malaysia is a tropical country that is relatively rich in water resources with an average annual rainfall of 2562.35 mm over the study area from 2007 to 2016 (Tan, 2018). Although Malaysia has never experienced any serious water crisis in the past few decades, uneven distribution of rainfall over space and time has led to some areas suffering from dry spells, while others have been affected by major flooding (Hafizi Md Lani et al., 2018). These facts reveal that RWH in Malaysia as a promising alternative water resource and flash flood reduction is crucial and has a high potential. Malaysia's climate is characterized by three main components namely temperature, wind pattern, and rainfall (Bahari et al., 2017). In this section, wind and rainfall patterns are described as the main parameters affecting the WDR phenomenon.

#### 2.2.1 Wind

The winds over the country are generally light and variable. There are, however, some uniform periodic changes in the wind flow

WDR permeates through the panel into the box and flows into the scale 1 via an outlet hose, and the Rainwater Runoff that flows down on the outer of the mesh surface leads into another gutter and is measured by scale 2. The base consists of the main control unit; includes water-measuring scales, and a bulky volume (1000 mm x 970 mm x 300 mm) made out of cement particleboard covered in aluminum sheeting to ensure the stability of the base in windy outdoor conditions.

patterns. Northeasterly winds prevail during the boreal winter monsoon (locally known as the northeast monsoon) from November to March. Southwesterly winds prevail during the boreal summer monsoon (locally known as the southwest monsoon) from May to September (MESTECC, 2018). These monsoons are separated by two shorter inter-monsoon periods.

#### 2.2.2 Rainfall

Rainfall is characterized by two rainy seasons associated with the southwest monsoon (SWM) from May to September and the northeast monsoon (NEM) from November to March (Suhaila et al., 2009; Tangang, 2001). The monsoon winds and topography are likely the main factors controlling the magnitude of the spatial rainfall variation in the country (Wong et al., 2016). The Titiwangsa Range is a mountain range that forms the backbone of the Peninsula. During the northeast monsoon (NEM), stronger winds blow to the exposed areas, e.g., the east coast of Peninsular Malaysia (Camerlengo et al., 1997; Juneng et al., 2007; Lim et al., 2013), thus these areas receive a substantial high amount of rainfall. Higher wind speeds promote more evaporation, which destabilizes the boundary layer and triggers deep convection, and hence, increases rainfall (Back et al., 2005). These features have enabled Malaysia to be blessed with abundant annual rainfall, with an average ranging from about 2,000 mm to 4,000 mm (MESTECC, 2018). During the southwest monsoon and the inter-monsoon periods, heavy rain from convective showers and thunderstorms occur in the late afternoons and evenings. Figure 9 shows the annual rainfall for Peninsular Malaysia from 1951 to 2015 (MESTECC, 2018). For this period, there is a very slight decreasing trend in the rainfall for Peninsular Malaysia. For a shorter time frame from 1990 onwards, increasing trends in rainfall are observed for Peninsular Malaysia.

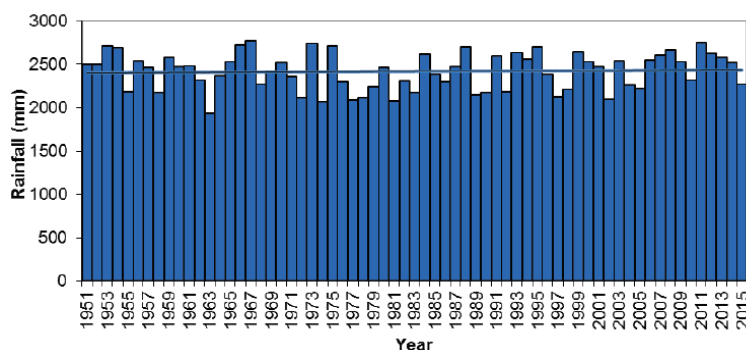


**Figure 9** Annual rainfall trends for Peninsular Malaysia, source: (MESTECC, 2018)

### 2.2.3 Weather in 2017

In 2017, the climate in Malaysia was greatly influenced by the natural climate variability due to normal weather conditions and neutral ENSO (Bahari et al., 2017).

ENSO index was neutral starting from January 2017 till the end of November 2017. A weak La Niña condition started in December 2017. Throughout 2017, Malaysia did not experience long-lasting hot and dry weather (Bahari et al., 2017). The haze phenomenon, drought, and heatwave also did not happen. Table 2 illustrates the period of seasons experienced in Malaysia in 2017.

**Table 2** Periods of seasons in Malaysia in 2017. Data derived from (Bahari et al., 2017)

Seasons	Duration
Monsoon Transitional Period	April 2017 to 16 <sup>th</sup> May 2017
Southwest Monsoon	17 <sup>th</sup> May 2017 to 5 <sup>th</sup> October 2017
Monsoon Transitional Period	6 <sup>th</sup> October to 12 <sup>th</sup> November 2017
Northeast Monsoon	13 <sup>th</sup> November to 27 <sup>th</sup> March 2018

In 2017, most of the stations recorded a consistent average wind speed compared to the long-term average (Bahari et al., 2017). Generally, throughout the year 2017, Malaysia has experienced normal weather and climate conditions.

### 2.3 UM WDR Gauge: Design and Installation

As previously stated, to date WDR gauges have not been industrially produced; there are various types of gauges that researchers applying for their measurement purposes. Table 1 presented 7 types of WDR gauges with differences in shape,

dimensions, material, function, and the accuracy of measurements.

The WDR gauge for this experimental study was manufactured at the University of Malaya (UM), Kuala Lumpur, Malaysia based on the gauge comparison results derived from the literature review and the goal of this research. In the study carried out by Blocken et al. (2005a) to design a WDR gauge, five possible error sources were presented. Table 3 shows the modifications and arrangements have been made to reduce errors and minimize the biases in the measurement process for the present experimental research:

**Table 3** Possible error sources while designing WDR gauge and modifications to minimize

No.	Possible error sources (Blocken et al., 2005a)	Modifications / Arrangements (by author)
1	adhesion-water evaporation	All parts of the gauge have been made of Acrylic sheets as an integrated device to promote water runoff.
2	evaporation from the reservoir	The bucket was covered with plastic between the upper cover and the bucket.
3	splashing of drops from the collection area	The catchment area is 20 x 20 cm <sup>2</sup> , and the rime around it has a height of 3 cm to minimize splashing from in and out of the gauge.
4	condensation on the collection area	Measurement has been done right after the rain stopped.
5	wind errors	The rime height around the gauge has been increased by 1 cm compared to the EMPA gauge to decrease wind error.

1. All parts of the WDR gauge collector at UM were made of a 10 mm Acrylic sheet and assembled heat pressing to avoid any drop leaking from the possible gaps. The material allows the rainwater drips down into the tube with the least possibility of water adhesion on the surface compared to the materials have been applied in the literature (Aluminium, Plate, Polytetrafluoroethylene, Stainless steel) and the size of collector area according to the recommendation by (Blocken et al., 2005a, 2005b, 2006a) was considered 20 x 20 cm<sup>2</sup> to reduce the evaporation.
2. To minimize evaporation from the reservoir, it was covered by two layers: (1) a plastic layer from inside to avoid water absorption and ventilation (2) a square shape plywood surface from outside to avoid solar radiation losses.
3. The collection area is 20 x 20 cm<sup>2</sup> to reduce the rate of water splashing because the bigger collector area the more rate of splashing error occurs. The height of rim around the collector area was increased 1 cm compared to the EMPA model to reach 3

cm height in order to minimize water splashing either from inside or outside the catchment area and also the possibility of entering water run-off from the surrounding area of the gauge.

4. The connector part to the tube has the same material as the collector and integrated to the collector via two internal slop surfaces. These surfaces allow the effective shedding of runoff rainwater from the catchment area into the tube and the reservoir respectively. The tube is a rubber-hose sealed from both external sides to the connector and the reservoir cover, and the reservoir is an ordinary bucket with a volume of 15 Litres. The length of the tube is at the shortest possible length located outside the building on the facade, buckets are also located outside the building along with the WDR gauges; in a tropical climate, normally there is no water freezing possibility even in the rainy days.

5. To reduce the wind error, (1) the area of the collector was designed at the practical minimum size based upon the previous studies, and (2) the height of rime around the gauge has been considered 3 cm (Figure 10).

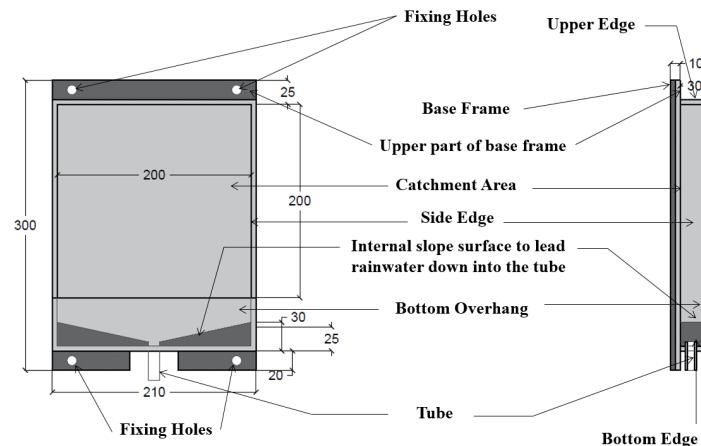


**Figure 10** Elevation and section of the WDR gauge collector. Dimensions (in mm).

#### 2.4 Pilot Building and Building Site

Figure 11 illustrates an aerial view of the measurement site. The building has dimensions  $L \times W \times H = 18.60 \times 6.40 \times 3.50$  m<sup>3</sup>. The long side is facing the northeast and exposed to a downhill open space. The southwest side is facing a pilot parking lot at 13

m distance, on its southeast and northwest sides are open parking area and the closest adjacent buildings are at 19.50 m and 25.70 m distance respectively. Different types of adjacencies around the building have made it a favorable building for wind-driven rain measurement study at the campus in an urban area.



**Figure 11** Aerial view of the building site

2.5 *Experimental Method*

2.5.1 WDR Measurement

Eight WDR gauges were installed on the facades of the pilot building at the campus of UM. The building is a flat-roof with no overhang. Kubilay et al. (2014) stated that the WDR distribution on the building facades shows the highest catch ratio values belonged to the top corners and the least values to the middle-

lower two-third of the facade. Accordingly, the present study installed WDR gauges on 4 facades of the building; 2 on each facade; one on top corner edge (2.75 m height) and one on middle two-third of the facade height (1 m height) to receive and measure the maximum and minimum accumulated WDR impinging into the gauges (Figure 12). The amount of WDR was collected by the reservoirs were measured manually immediately after the rain stopped every day.

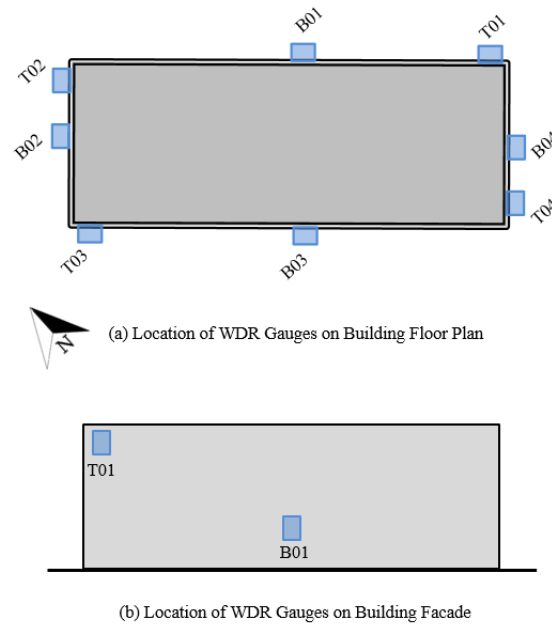


**Figure 12** The orientation of the pilot building and locations of the WDR gauges on the building: (a) Floor plan and (b) the facade (not to scale).

2.5.2 Meteorological Data Measurement

A meteorological mast was installed at 3.50 m height to measure the on-site wind direction, wind speed, and wind gust (Figure

13). Its location is at the nearest point to the building model and also out of the constant flux layers around the buildings in an open area to obtain the actual data recorded.



**Figure 13** The pilot building and position of the WDR gauges on the facades (a) South view (b) Meteorological mast on the roof of the building at the parking area.

### 3. Measurement Results

A year measurement was conducted and categorized during four periods of tropical seasons experienced in Malaysia based on Table 2 in 2017. The first period was from April to 16th May 2017 as the First Monsoon Transitional Period. The second period of measurement was from 17th May to 5th October 2017; Southwest Monsoon season, and the third period was from 6th October to 12th November 2017: the Second Monsoon Transitional Period. The fourth and last season of measurement was 13th November to 27th March 2018 as the Northeast Monsoon season.

Figure 14 illustrates an overview of 94 WDR events measured by 8 wall-mounted gauges (top corner and lower middle of the facades) over the 4 tropical seasons of Malaysia. As the annual

report of UNFCCC (2015) on the rainfall trends in Kuala Lumpur declared that rain occurs mostly in the afternoons and evenings, in this study, nocturnal precipitation (12 a.m. to 6 a.m.) and also those diurnal accumulated precipitations with the amount of fewer than 1 ml were excluded from the record. The total duration of the monitored rain events over the 4 periods in this experimental research was 7115 minutes (~119 hrs.).

The following subsections consist of the meteorological data and cumulative WDR of each season period, categorized in 4 seasons. Each season is presented with (i) table of wind speed, wind direction, wind gust, rainfall duration time, horizontal rainfall, and rainfall intensity measured by the meteorological mast installed at the site, and (ii) graph of cumulative WDR manually measured by the 8 wall-mounted gauges installed on the building facades.

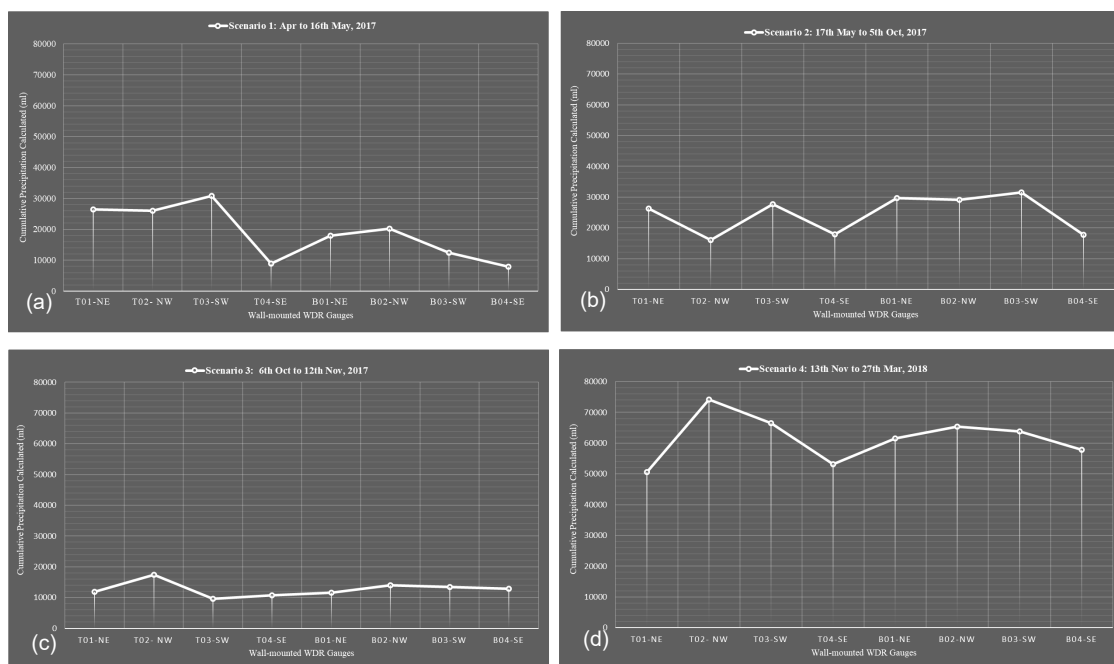


**Figure 14** Cumulative precipitation calculated on the basis of Season 1: April to 16th May 2017 (a), Season 2: 17th May to 5th October 2017 (b), Season 3: 6th October to 12th November 2017 (c), and Season 4: 13th November to 27th March 2018 (d).

#### 3.1 Season 1: Monsoon Transitional Period; April to 16th May, 2017

The meteorological data record of reference wind speed, reference wind direction, wind gust, horizontal rainfall intensity, and rainfall duration from April to 16th May 2017 during the daily rain events is shown in Table 4. The number of rainy days in this

period is 14 days with a precipitation duration of 1210 minutes. The total horizontal rainfall amount is 35.72 mm, mostly less than 2 mm/hr, and only one occasion is reached 11.6 mm/hr. The wind speed fluctuating between 1-6 km/hr, the wind gust between 2-8 km/hr, and the wind direction is mostly west-southwest, almost normal to the building surface

**Table 4** The meteorological data record of Monsoon Transitional Period; April to 16<sup>th</sup> May 2017

Date	Rainfall Duration Time (min)	Wind Speed (km/h)	Wind Direction	Wind Gust (km/h)	Horizontal Rainfall intensity (mm/hr)
21-Apr-16	150	5	WNW	8	1.25
23-Apr-16	135	4	W	6	3.34
24-Apr-16	60	4	SW	5	4.7
25-Apr-16	20	5	SE	6	0.59
26-Apr-16	65	4	SW	5	2.1
28-Apr-16	30	6	SW	8	0.99
29-Apr-16	175	3	ENE	5	3.27
30-Apr-16	45	6	NW	8	1.33
2-May-16	60	5	SW	7	2.78
5-May-16	110	4	NNE	8	1.59
7-May-16	165	3	WNW	6	5.9
10-May-16	60	1	WSW	2	1.28
12-May-16	105	4	NNW	8	0.8
13-May-16	30	4	WSW	6	5.8

Figure 14(a) shows the cumulative precipitation calculated from 8 WDR gauges over 1st monsoon transitional period of the year. As the figure illustrates the gauges T03-SW among top gauges and the B02-NW among the bottom ones have received the highest amount of WDR; (i) the wind direction is mainly from west to southwest (ii) the longest duration of daily rainfall belongs to the events with north directions (T01-NE, T02-NW, B01-NE, B02-NW). The average wind speed for both SW and N directions is almost equal (Table 4).

### 3.2 Season 2: Southwest Monsoon; 17th May to 5th October, 2017

The meteorological data record for the rain event on 17th May to 5th October 2017 is shown in Table 5. The number of rainy days in this period is 22 days with a precipitation duration of 1495

minutes. The total horizontal rainfall amount is 45.03 mm, mostly less than 2 mm/hr and a few occasions between 3 to 6 mm/hr intensity. This rain event has wind speed and a wind gust of more than 1.5 times the ones in the previous season; the wind speed fluctuating between 3-10 km/hr, the wind gust between 4-12 km/hr. The main wind direction in this season, as its name implies and the weather station was recorded, is west-southwest (Table 5).

Figure 14(b) illustrates the cumulative precipitation calculated from 8 WDR gauges over Southwest Monsoon. As the figure illustrates the gauges T03-SW among top gauges and the B03-SW among the bottom ones have received the highest amount of WDR; (i) both from the southwest facade facing the prevailing wind direction of west to the southwest over this season.

**Table 5** The meteorological data record of Southwest Monsoon; 17<sup>th</sup> May to 5<sup>th</sup> October 2017

Date	Rainfall Duration Time (min)	Wind Speed (km/h)	Wind Direction	Wind Gust (km/h)	Horizontal Rainfall Intensity (mm/hr)
20-May-16	40	6	SW	7	1.37
23-May-16	25	7	NNW	8	0.66
25-May-16	25	5	NNW	8	2.39
3-Jun-16	80	6	E	4	2.72
9-Jun-16	90	7	NW	10	4.6
11-Jun-16	60	3	WNW	6	2.78
12-Jun-16	60	4	NNE	8	3.22
14-Jun-16	25	6	WNW	8	2.75
17-Jun-16	40	10	ESE	12	1.24
19-Jun-16	90	4	NNE	7	3.15
11-Jul-16	45	7	WSW	8	0.35
12-Jul-16	20	5	SSW	8	1.98
13-Jul-16	110	6	WSW	7	1.15
14-Jul-16	80	8	SW	10	0.16
20-Jul-16	75	7	SSW	8	0.39
21-Jul-16	90	7	S	8	0.85
22-Jul-16	90	7	SW	8	0.95
11-Aug-16	60	8	WNW	10	0.73
23-Aug-16	105	4	WNW	7	0.25
30-Aug-16	105	4	ESE	7	4.72
31-Aug-16	60	8	SSW	10	5.45
1-Sep-16	120	5	SSW	8	7.59

Note that, the average daily rainfall duration of this season (67 min) is lower than the season 1 (86 min), while its average horizontal rain (49.45 mm) is higher than season 1 (35.72 mm), and also its accumulated WDR amount (195,978 ml) is much higher than the season 1 (150,489 ml). Consequently, even though the average rainfall duration is lower than the previous season but the wind speed has been stronger with more consistent wind direction and thus accumulated more horizontal and wind-driven rain over this season.

### 3.3 Season 3: Monsoon Transitional Period; 6th October to 12th November, 2017

The meteorological data record for the rain event from 6th October to 12th November 2017 is shown in Table 6. The number of rainy days in this period is 13 days and the precipitation duration is 1090 minutes which are shorter than both previous seasons.

The total horizontal rainfall amount is 20.43 mm, mostly less than 1.5 mm/hr and only one occasion with 5 mm/hr intensity. This

rain event has wind speed and a wind gust of even more than season 2; the wind speed fluctuating between 2-14 km/hr, the wind gust between 3-17 km/hr, but the horizontal rainfall amount is less than half of the season 2. This season is a shorter one, and more homogeneous in terms of wind speed values and wind directions; wind direction fluctuations display a more isotropic distribution (Table 6). During the first half (October), the wind speed is high and daily rainfall duration is low. In the second half (November), wind speed decreases, daily rainfall duration increases, and rainfall intensity is relatively higher and homogeneous. The wind direction is mostly from west fluctuating from Northwest in October to Southwest in November.

Figure 14(c) shows the cumulative precipitation calculated from 8 WDR gauges over the 2nd monsoon transitional period of the year. As the figure indicates the gauges T02-NW among the top gauges and the gauge B02-NW among the bottom gauges on the facade have collected the highest amount of WDR during this season. The figure also indicates there are not noticeable sharp differences between the rest of gauges in terms of accumulated WDR amount and the graph has a homogeneous trend in general

**Table 6** The meteorological data record of Monsoon Transitional Period; 6<sup>th</sup> October to 12<sup>th</sup> November 2017

Date	Rainfall Duration Time (min)	Wind Speed (km/h)	Wind Direction	Wind Gust (km/h)	Horizontal Rainfall Intensity (mm/hr)
12-Oct-16	40	14	WNW	17	0.58
16-Oct-16	75	12	NW	14	0
24-Oct-16	60	5	NW	10	0.11
25-Oct-16	30	11	NW	13	0.67
27-Oct-16	35	4	W	6	2.95
29-Oct-16	195	6	WNW	9	1.16
3-Nov-16	60	6	W	8	1.09
6-Nov-16	40	4	W	4	0.15
7-Nov-16	45	6	WSW	9	1.23
9-Nov-16	180	7	SW	8	4.41
10-Nov-16	120	4	WSW	7	3.76
11-Nov-16	150	2	SW	3	2.19
12-Nov-16	60	4	WNW	7	2.13

### 3.4 Season 4: Northeast Monsoon; 13<sup>th</sup> November to 27<sup>th</sup> March, 2018

The meteorological data record for the rain event on 13<sup>th</sup> November to 27<sup>th</sup> March 2017 is shown in Table 7. The number of rainy days in this period is 44 days and the precipitation duration is 3845 minutes which are the highest compared to the previous 3 seasons of the year.

The total horizontal rainfall amount is 60.76 mm, mostly less than 1 mm/hr and a few occasions between 2 to 5 mm/hr intensity. Hence this season consists of average daily rainfall duration (87 min) almost the same as season 3 (83 min) but in the longest period (44 days and 3845 min) which resulted in a sharp increase in the amount of horizontal rainfall. This rain event has wind speed and a wind gust of about the same as season 3; the wind speed fluctuating between 1-13 km/hr, and the wind gust

between 2-15 km/hr. The wind direction in this season, as its name implies and the weather station was recorded, is mostly northeast and northwest respectively and short periods switches to the southwest.

Figure 14(d) shows the cumulative precipitation calculated from 8 WDR gauges over the northeast monsoon period. The maximum annual precipitation duration along with the effective wind speed during this season leads to the highest cumulative WDR amount with the maximum difference compared to the previous seasons. However, the main wind direction is northeast but the gauges facing northwest and southwest (T02-NW, T03-NW, B02-SW) have accumulated more WDR amount during this season. Two factors have influenced this result; (i) the precipitation duration, and (ii) wind speed which have been more variable in terms of their values (Table 7) in contrary to the season 3 as the most homogeneous season.

**Table 7** The meteorological data record of Northeast Monsoon; 13<sup>th</sup> November to 27<sup>th</sup> March 2018

Date	Rainfall Duration Time (min)	Wind Speed (km/h)	Wind Direction	Wind Gust (km/h)	Horizontal Rainfall Intensity (mm/hr)
13-Nov-16	60	3	N	6	1.8
15-Nov-16	70	3	S	4	1.32
18-Nov-16	180	5	NW	8	6.24
24-Nov-16	45	1	WSW	2	3.43
25-Nov-16	135	4	SSW	4	1.1
27-Nov-16	150	2	W	3	3.4
28-Nov-16	120	3	SW	3	0.11
29-Nov-16	165	7	NE	12	1.42
1-Dec-16	50	3	WNW	5	0.56
2-Dec-16	105	5	NW	6	0.9

3-Dec-16	70	5	NW	7	1.23
9-Dec-16	35	2	NW	2	1.38
10-Dec-16	50	6	NW	8	1.23
13-Dec-16	60	13	WNW	15	0
17-Dec-16	90	3	ENE	5	4.44
19-Dec-16	55	7	W	9	2.53
25-Dec-16	100	5	NE	8	4.35
26-Dec-16	105	4	NNE	7	1.08
27-Dec-16	50	5	ENE	8	0.4
31-Dec-16	75	4	NE	6	0.03
3-Jan-17	80	5	ENE	11	1.02
17-Jan-17	90	4	SW	6	2.22
19-Jan-17	165	3	SSW	6	1.56
20-Jan-17	105	4	WSW	5	5.44
23-Jan-17	45	4	NE	7	0.05
24-Jan-17	30	4	WNW	6	2.84
25-Jan-17	40	4	SSW	5	2.16
26-Jan-17	50	1	NE	2	0.15
28-Jan-17	80	2	WNW	3	0.7
30-Jan-17	45	3	SE	3	0.38
4-Feb-16	175	3	NW	6	0
5-Feb-16	100	6	SSW	10	0.77
15-Feb-16	150	5	ENE	10	1.3
18-Feb-16	25	5	E	10	0
19-Feb-16	170	1	ENE	3	0.24
22-Feb-16	130	2	ENE	5	0
23-Feb-16	140	5	NNE	6	0.02
28-Feb-16	40	4	NNE	7	0.65
4-Mar-16	85	5	NW	10	0
8-Mar-16	55	3	WNW	5	0.44
10-Mar-16	20	5	W	6	0.33
13-Mar-16	150	2	WSW	3	2.66
15-Mar-16	45	5	NNW	6	0.88
16-Mar-16	60	5	NNE	7	0

#### 4. Discussion

The building site enables this research to experiment 3 different adjacency to the pilot building, the windward facades has/have: (i) no adjacent building, facing a downhill; wind flows freely with no obstruction (NE facade), (ii) a one-story adjacent building (same height as the pilot building) at 19.50 m (SE facade) and 25.70 m distance (NW facade) in an open parking area; windflow obstructs slightly by other buildings and trees, (iii) a pilot parking of a 10-story adjacent building at 13 m distance; wind flows with more obstruction in presence of the tall building (SW facade). Since the aim of this study is quantifying WDR loads on vertical facades of the urban buildings as an alternative water resource in the RWH system, this variety of the surrounding areas provides a real scenario similar to an urban building location and orientation with different levels of adjacency of surrounding buildings and landscapes. The WDR database derived from this measurement provides a direct indication of WDR quantification loads on building facades as the scope of this paper, and also as a crucial requirement for the development and validation of models that will be addressed in future research topics.

Comparison between WDR distribution on the building facades and calculated cumulative precipitation in all 4 seasons (Table 8 & Figure 15) show:

- i. The NE facade has almost always received a noticeable amount of WDR even when wind direction has not been aligned with the facade orientation such as during seasons 1 and 2. The reason is the location of this facade which is facing a downhill open space with no obstacle in the surrounding area to distract or decrease the wind direction or speed value.
- ii. Comparison between WDR catch ratio values of the top and bottom gauges shows despite the expectations from previous studies that top corner gauges would collect higher amounts than the bottom middle ones (section 2.5.1), 3 out of 4 seasons the bottom middle ones have received a higher amount of WDR. Only over season 1, the top gauges received 33,615 ml more than bottom gauges (61%). However, over seasons 2, 3, and 4 the bottom gauges received respectively 20,318 ml (55%), 2,368 ml (51%), and 4,109 ml (50%) more than the top gauges.
- iii. NW and SW are among the directions with the highest catch ratio values in almost all the seasons. According to the

results, these two directions are considered as the prevailing wind directions with the largest wind speed values over a year.

iv. The 2nd transitional monsoon, season 3, with the minimum number of rainy days (13 days), and total horizontal rainfall (20.43 mm) has cumulated the lowest amount of WDR (101,428 ml). This season is the shortest event (1090 min) with the most homogeneous flow of the wind in direction, velocity, and rainfall intensity (Table 8).

v. Northeast monsoon, season 4, with the maximum number of rainy days (44 days), highest average daily rainfall duration time (87.38 min) and total horizontal rainfall (60.76 mm) has remarkably cumulated the highest amount of WDR (493,065 ml), more than twice-fifth times each of the other three seasons (Table 8).

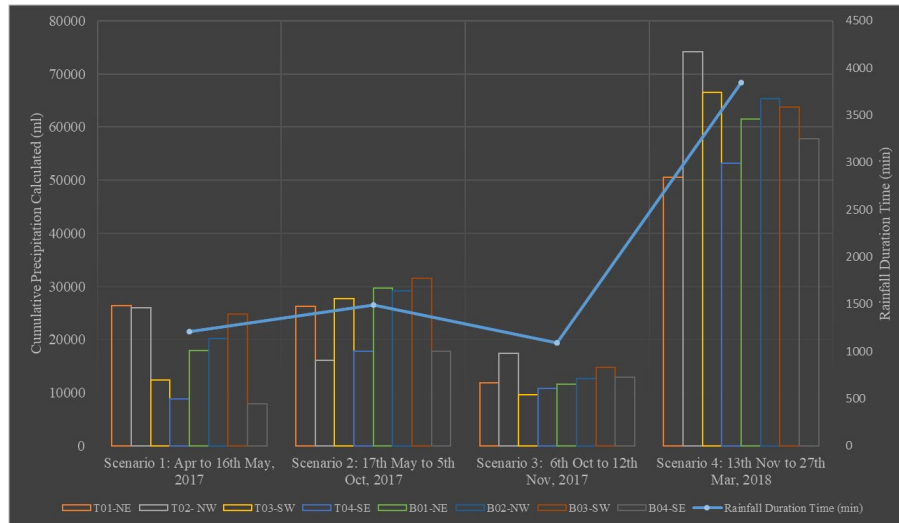


**Figure 15** 12 months measurements of WDR (ml) of 93 events divided into 4 tropical seasons by 8 wall-mounted gauges; installed on the top corner and lower middle of the facades (April 2017 - March 2018)

**Table 8** Seasonal variation of meteorological data derived from the mast and WDR gauges of 83\* events (April 2017 - March 2018)

Seasons Over A Year	Horizontal Rainfall Intensity $R_h$ (mm/hr)	$R_h^{0.88}$	Wind Speed $U$ (m/s)	$B \times H \times U \times R_h^{0.88}$	In-situ Cumulated WDR (mm/hr)	Constant $\gamma$
Season 1: Apr to 16th May, 2017	29.74	19.80	1.23	7.79	7.27	0.93
Season 2: 17th May to 5th Oct, 2017	48.21	30.28	1.64	15.89	7.70	0.48
Season 3: 6th Oct to 12th Nov, 2017	16.23	11.61	1.36	5.05	3.68	0.73
Season 4: 13th Nov to 27th Mar, 2018	54.49	33.72	1.10	11.87	7.58	0.64

\*All variables were subjected to the normality test (through IBM SPSS Statistic 26 software)

#### 4.1 Application Of Empirical Equation To Validate The Measured Data

As Blocken et al. (2005b) stated that experimental data are used for model development and validation, in this section the in-situ measurement data collected in 4 tropical seasons are exploited to determine WDR coefficient ( $\gamma$ ) to estimate the amount of WDR on a building façade via an empirical WDR relationship. WDR

relationships are frequently used as a tool to calculate WDR amount on building facades (Blocken et al., 2004, 2005b). In this study, the equation that has been developed by Cho et al. (2020) will be referred to:

$$Q = \gamma \times B \times H \times U \times R_h^{0.88} \quad \text{Equation 1}$$

where  $Q$  is the sum of rainfall over the building façade (WDR), constant  $\gamma$  is the WDR coefficient,  $B$  and  $H$  represent the building width (m) and height (m) respectively,  $U$  is the horizontal wind speed (m/s),  $R_h$  is the rainfall intensity (mm/hr). WDR rain equation globally is used not only to calculate WDR amount but also a wide range of Heat-Air-Moisture (HAM) transfer simulation programs (Blocken et al., 2005b) and also the European Standard Draft (CEN, 2009) have employed it in their calculation and assessment processes.

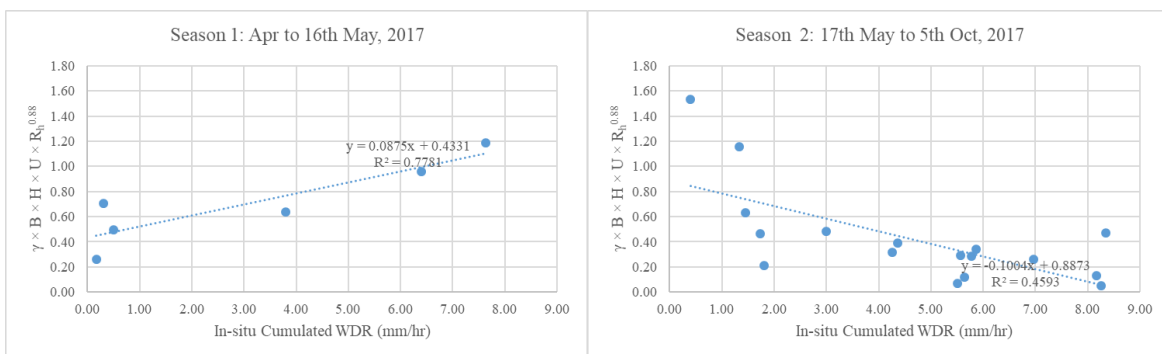
The constant  $\gamma$  is determined from hourly measurements of wind speed, horizontal rainfall intensity, area of WDR gauges, and WDR collected from in-situ measurement. Table 8 shows the total amount of WDR collected by 8 gauges in 4 different tropical seasons. The constant  $\gamma$  was calculated by comparing  $B \times H \times U \times R_h^{0.88}$  value with cumulated in-situ WDR amount. Due to unique rainfall and wind patterns in the tropical climate, the calculation process has been conducted individually for each season and as indicated in the table the values differ from 0.48 to 0.98. In the literature, the minimum value for constant  $\gamma$  has been calculated as 0.02 by Lacy (1965) and Hens et al. (1994), and maximum as 0.26 by (Flori, 1992). According to the literature, the calculated values of  $\gamma$  in this study can be considered significantly high. The correlation between observed and calculated WDR amounts in all seasons also illustrate low  $R$ -squared values (Figure 16) ranging from 0.17 to 0.77. But the reasons for these high  $\gamma$  and low  $R^2$  values could be explained by potential sources/possibilities affecting the values in this particular climate:

- Constant  $\gamma$  in equation 1 which has been developed under lab-observations (Cho et al., 2020), is a function of time, due to its dependency on wind speed, wind direction, and also rainfall intensity (Blocken et al., 2006b), and in a real measurement it is difficult to

define particular values for the aforementioned parameters.

- Errors in observation are variable in time, particularly in heavy or prolonged precipitation which are main characteristics of tropical rainfall pattern; it has been illustrated in the data record of season 4 (Table 7) comprising the highest numbers of daily long-term precipitations (mostly more than one hour) and lowest  $R^2$  value of 0.17 accordingly (Figure 16). However, this equation has been developed to estimate WDR amounts based on the hourly experimental data for  $U$  and  $R_h^{0.88}$ .
- Another parameter affecting the amount of WDR impinging on the wall in reality, is the wind gust speed which has not been considered in the equation, while makes a significant impact on the discrepancies between observed and calculated values.
- Equation 1 has considered all 4 walls of the typical building equally to estimate the amount of impinged WDR, however in reality WDR impinged on one or two façade(s) at a particular time based on the fluctuation of wind direction and also the orientation of the exposed walls.
- Therefore, the constant  $\gamma$ , in this study can be referred to as approximate estimation.

As a result and as Figure 16 clarifies the real-time variation of the constant  $\gamma$  and the in-situ measurement errors have resulted in the low  $R^2$  values which indicates a low correlation between observed and calculated amounts of WDR. Seasons with larger rainfall durations such as seasons 2 and 4 have been encountered with more discrepancies. And on the other hand, seasons 1 and 3 claim that the equation and constant  $\gamma$  can be considered a valid tool to estimate the amount of WDR.



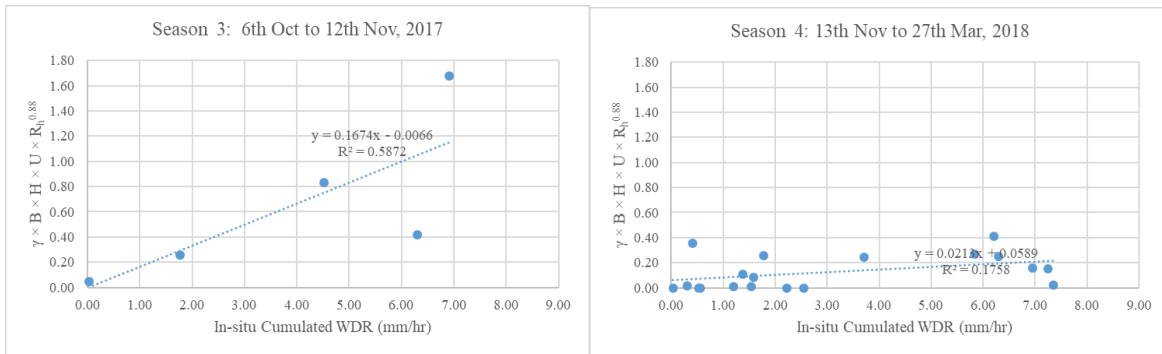


**Figure 16** Determination of R-squared value ( $R^2$ ) of in-situ cumulated WDR and calculated WDR correlation based on equation 1 for each of 4 tropical seasons

In lab-observation, lower discrepancies are recorded, but as Blocken et al. (2005b) stated in reality [such as this study], larger discrepancies are unavoidable. Further research will specifically focus on the performance of this equation on each building façade in shorter periods of precipitation.

## 5. Conclusion

This research followed principles of the WDR field measurement method in building science. The WDR measurement was conducted on a single story pilot building in the tropical climate of Kuala Lumpur. The building was instrumented with 8 WDR gauges; 2 on each facade. This paper presented the principle guidelines to design and manufacture the gauge, description of the building, surrounding area, results of the one-year measurement of meteorological data and WDR, and also an empirical equation to validate the data. Topography and monsoon winds as the main factors impact the flow of the wind direction and velocity and consequently the WDR loads on building facade. However, the effectiveness of the wind depends on the monsoon characteristics which are not constant and vary in different seasons, but some seasons are individually nearly homogeneous. This character of the wind plays an important role in applicability of the equation because it directly affects the constant  $\gamma$  value. Although 93 rain events data during one-year have been measured, but after data processing and normalization test (through IBM SPSS Statistic 26 software) prior to determine the constant  $\gamma$ , 10 events were excluded. And to calculate  $R^2$  also only 43 events were considered as normal values for calculations based on normality test results.

It must be noted that wind guest speed which is mostly higher than wind speed in this climate as can be seen in tables 4-7, has a major contribution to the amount of cumulated WDR but has not been considered in the equation. It is necessary to assess and analyze its influence as another independent value in the calculation of WDR in future studies.

Referring to the lab-experiment by Cho et al. (2020), building walls can collect 50% more rainwater than roof area if the wall/roof ratio is only one, and when the ratio is 10 the amount of cumulated rainwater is higher even if the wind speed would be

1 m/s. On the other hand, as mentioned previously roof areas are no longer available in modern urban areas for the RWH system.

In this regard, the current real-time measurement from the vertical building façades proved the high potential and feasibility of WDR collection as an alternative water resource for the RWH system. 8 WDR gauges ( $8 \times 0.04 \text{ m}^2$ ) were installed on 4 different facades and collected 26.23 mm/hr rainwater; which is equivalent to about 2,600 liters/ $\text{m}^2$ /year from building facade. According to the Malaysian Water Association (MWA, 2018), Malaysia needs to reduce its high water-usage (201 liters/capita/day) by 18% to reach the recommended water-usage by World Health Organization (WHO), i.e. 165 liters/capita/day. On the other hand, Bari et al. (2015) survey results revealed that 29% of household water consumption accounts for non-potable activities (toilet flushing and gardening). In conclusion, each square meter of vertical façade area has the capability to supply 12% of non-potable or 4.9% of potable water-usage per capita per day in the tropical climate of Malaysia.

The authors hope the present paper will stimulate further attempts in academia to promote industry's interest in vertical RWH from facades of growing high-rise buildings in urban areas as a new and more effective approach to harvest rainwater in comparison with the traditional horizontal RWH from rooftop or ground surfaces.

## Acknowledgement

This work was supported by the Institute of Research Management & Services (IPPP), Research Management & Innovation Complex, University of Malaya, Kuala Lumpur, Malaysia [grant number: RG317-14AFR].

## References

- Adriano, T. E., Antonio, E. M., Rodolfo, G. N., & Mme. (2011). Rainwater Harvesting, Quality Assessment And Utilization In Region I E-International Scientific Research Journal 3(2), 145-155. [http://www.eisrjc.com/documents/Rainwater\\_Harvesting\\_1325914607.pdf](http://www.eisrjc.com/documents/Rainwater_Harvesting_1325914607.pdf)

- Back, L. E., & Bretherton, C. S. (2005). The relationship between wind speed and precipitation in the Pacific ITCZ. *Journal of climate*, 18(20): 4317-4328. doi:<https://doi.org/10.1175/JCLI3519.1>
- Bahari, Y. A. b., Pengarah, K., & Malaysia, J. M. (2017). Jabatan Meteorologi Malaysia, Annual Report 2017. Malaysia: Jabatan Meteorologi Malaysia Retrieved from [https://www.met.gov.my/content/pdf/penerbitan/laporantahunan/la\\_porantahunan2017.pdf](https://www.met.gov.my/content/pdf/penerbitan/laporantahunan/la_porantahunan2017.pdf). Retrieved on 17/02/2020
- Bari, M., Begum, R. A., Nesadurai, N., & Pereira, J. J. (2015). Water consumption patterns in greater Kuala Lumpur: potential for reduction. *Asian Journal of Water, Environment and Pollution*, 12(3): 1-7.
- Beorkrem, C., & Damiano, A. (2018). [Kak-Tos]: A Tool for Optimizing Conceptual Mass Design and Orientation for Rainwater Harvesting Facades *Humanizing Digital Reality* 603-612. Springer.
- Blocken, B., & Carmeliet, J. (2004). A review of wind-driven rain research in building science. *Journal of Wind Engineering and Industrial Aerodynamics* 92: 1079–1130. doi: <https://doi.org/10.1016/j.jweia.2004.06.003>
- Blocken, B., & Carmeliet, J. (2005a). *Guidelines for wind, rain and wind-driven rain measurements at test-building sites*. Paper presented at the Proceedings of the 7th Symposium on Building Physics in the Nordic Countries: Reykjavik. <https://research.tue.nl/en/publications/guidelines-for-wind-rain-and-wind-driven-rain-measurements-at-tes>
- Blocken, B., & Carmeliet, J. (2005b). High-resolution wind-driven rain measurements on a low-rise building—experimental data for model development and model validation. *Journal of Wind Engineering and Industrial Aerodynamics*, 93(12): 905-928. doi: <https://doi.org/10.1016/j.jweia.2005.09.004>
- Blocken, B., & Carmeliet, J. (2006a). On the accuracy of wind-driven rain measurements on buildings. *Building and Environment*, 41(12): 1798-1810. doi:<https://doi.org/10.1016/j.buildenv.2005.07.022>
- Blocken, B., & Carmeliet, J. (2006b). On the validity of the cosine projection in wind-driven rain calculations on buildings. *Building and Environment*, 41(9): 1182-1189.
- Camerlengo, A., & Demmler, M. I. (1997). Wind-driven circulation of peninsular Malaysia's eastern continental shelf. *Scientia Marina*, 61: 203-211. doi: <http://scimar.icm.csic.es/scimar/pdf/61/sm61n2203.pdf>
- Canavan, D. H. (2008). Facade rainwater harvesting system: Google Patents.
- CEN. (2009). Hygrothermal performance of buildings Climatic data Part 3: calculation of a driving rain index for vertical surfaces from hourly wind and rain data. Retrieved from <https://www.sis.se/api/document/preview/910850/>. Retrieved on 15/01/2020
- Cho, E., Yoo, C., Kang, M., Song, S.-u., & Kim, S. (2020). Experiment of wind-driven-rain measurement on building walls and its in-situ validation. *Building and Environment*, 185: 107269. doi:<https://doi.org/10.1016/j.buildenv.2020.107269>
- Connor, R. (2015). *The United Nations world water development report 2015: water for a sustainable world* (9231000713). Retrieved from <https://sustainabledevelopment.un.org/content/documents/1711Water%20for%20a%20Sustainable%20World.pdf>
- Dobravaliskis, M., Spūdys, P., Vaičiūnas, J., & Fokaides, P. (2018). Potential of harvesting rainwater from vertical surfaces. *Journal of Sustainable Architecture and Civil Engineering*, 23(2): 49-58. doi:<https://doi.org/10.5755/j01.sace.23.2.21606>
- FJR van Mook. (2002). *Driving rain on building envelopes* (906814569X). Retrieved from Eindhoven University Press, Eindhoven, The Netherlands: <http://fabien.galerio.org/drivingrain/fjrvanmook2002/>
- Flori, J. (1992). *Influence des conditions climatiques sur le mouillage et le sechage d'une facade verticale*: CSTB.
- Foroushani, S. S. M. (2013). A Numerical Study Of The Effects Of Overhangs On The Wind-Driven Rain Wetting Of Building Facades. (Master), Ryerson University, Toronto, Ontario, Canada. <https://doi.org/10.1016/j.jweia.2013.10.007>
- Hafizi Md Lani, N., Yusop, Z., & Syafiuddin, A. (2018). A review of rainwater harvesting in Malaysia: Prospects and challenges. *Water*, 10(4): 506. doi:<https://doi.org/10.3390/w10040506>
- Hens, H., & Ali Mohamed, F. (1994). Preliminary results on driving rain estimation, Contribution to the IEA annex 24, Task 2 Environmental conditions T2-B-94/02. Retrieved from <https://lib.ugent.be/en/catalog/rug01:000697882>. Retrieved on 20/03/2021
- Hogberg, A. (1998). *Microclimate description: to facilitate estimating durability and service life of building components exposed to natural outdoor climate*: Chalmers University of Technology.
- Hogberg, A. (1999). *Microclimate measurement focused on wind-driven rain striking building surfaces*. Paper presented at the Proc. of the 5th Symp. on building physics in the Nordic Countries, Gothenburg.
- Hogberg, A. (2002). *Microclimate Load: Transformed Weather Observations for Use in Durable Building Design*: Department of Building Physics, Chalmers University of Technology.
- Hogberg, A., Kragh, M., & van Mook, F. (1999). *A comparison of driving rain measurements with different gauges*. Paper presented at the Proceedings of the 5th Symposium of building physics in the Nordic Countries, Gothenburg. <http://citeseerx.ist.psu.edu/viewdoc/download?doi=10.1.1.606.3604&rep=rep1&type=pdf>
- Juneng, L., Tangang, F., & Reason, C. (2007). Numerical case study of an extreme rainfall event during 9–11 December 2004 over the east coast of Peninsular Malaysia. *Meteorology and Atmospheric Physics*, 98(1-2): 81-98. doi:<https://doi.org/10.1007/s00703-006-0236-1>
- Kragh, M. K., & Svendsen, S. (1998). Microclimatic conditions at the external surface of building envelopes. (Ph. D), Technical University of Denmark. Retrieved from <https://core.ac.uk/download/pdf/13738237.pdf>. Retrieved on 22/02/2017
- Kubilay, A., Derome, D., Blocken, B., & Carmeliet, J. (2014). High-resolution field measurements of wind-driven rain on an array of low-rise cubic buildings. *Building and Environment*, 78: 1-13. doi:<https://doi.org/10.1016/j.buildenv.2014.04.004>
- Lacy, R. (1965). Driving-rain maps and the onslaught of rain on buildings. Paper presented at the 2nd International CIB/RILEM Symposium on moisture problems in Buildings, August 16-19, 1965, Helsinki, Finland.

- Lade, O., & Oloke, D. (2015). Modelling Rainwater System Harvesting in Ibadan, Nigeria: Application to a Residential Apartment. *American Journal of Civil Engineering and Architecture*, 3(3): 86-100. doi:10.12691/ajcea-3-3-5 <http://pubs.sciepub.com/ajcea/3/3/5>
- Lim, E., Das, U., Pan, C., Abdullah, K., & Wong, C. (2013). Investigating variability of outgoing longwave radiation over peninsular Malaysia using wavelet transform. *Journal of Climate*, 26(10): 3415-3428. doi:<https://doi.org/10.1175/JCLI-D-12-00345.1>
- Masters, F. J., Gurley, K. R., Prevatt, D. O., Rivers, B., & Kiesling, A. (2013). Wind-Driven Rain Effects on Buildings, Task Committee on Wind-Driven Rain Effects, Environmental Wind Engineering Committee, Technical Council on Wind Engineering, ASCE (12-00005-00). Retrieved from [http://www.floridabuilding.org/fbc/commission/FBC\\_0613/HRAC/2012\\_2013\\_Task\\_3\\_Final\\_Report.pdf](http://www.floridabuilding.org/fbc/commission/FBC_0613/HRAC/2012_2013_Task_3_Final_Report.pdf). Retrieved on 15/01/2017
- MESTECC. (2018). Malaysia's Third National Communication and Second Biennial Update Report submitted to the United Nations Framework Convention on Climate Change in September 2018. Putrajaya, Malaysia: Ministry of Energy, Science, Technology, Environment and Climate Change Retrieved from [https://unfccc.int/sites/default/files/resource/Malaysia%20NC3%20B%20UR2\\_final%20high%20res.pdf](https://unfccc.int/sites/default/files/resource/Malaysia%20NC3%20B%20UR2_final%20high%20res.pdf). Retrieved on 16/03/2020
- MWA. (2018). Malaysia Water Industry Guide. Retrieved from The Malaysian Water Association, Kuala Lumpur, Malaysia: Retrieved on 22/03/2021
- SDI. (2003). *A Study on Preventing Flood Damage and Water Saving through Rainwater Utilization*. Seoul Development Institute, Seoul, Korea.
- Silva, C. M., Sousa, V., & Carvalho, N. V. (2015). Evaluation of rainwater harvesting in Portugal: Application to single-family residences. *Resources, Conservation and Recycling*, 94: 21-34. doi:<https://doi.org/10.1016/j.resconrec.2014.11.004>
- Suhaila, J., & Jemain, A. A. (2009). Investigating the impacts of adjoining wet days on the distribution of daily rainfall amounts in Peninsular Malaysia. *Journal of Hydrology*, 368(1-4): 17-25. doi:<https://doi.org/10.1016/j.jhydrol.2009.01.022>
- Tan, K. C. (2018). Trends of rainfall regime in Peninsular Malaysia during northeast and southwest monsoons. *Journal of Physics: Conference Series*, 995(1): 012122. doi:<https://doi.org/10.1088/1742-6596/995/1/012122>
- Tangang, F. T. (2001). Low frequency and quasi-biennial oscillations in the Malaysian precipitation anomaly. *International Journal of Climatology: A Journal of the Royal Meteorological Society*, 21(10): 1199-1210. doi:<https://doi.org/10.1002/joc.676>
- UNFCCC. (2015). Malaysia National Communication to The UNFCCC. Putrajaya, Malaysia: Ministry Of Natural Resources And Environment Malaysia Retrieved from <https://unfccc.int/resource/docs/natc/malnc2.pdf>. Retrieved on 22/03/2021
- Van Mook, F. (1998). Description of the measurement set-up for wind and driving rain at the TUE. Report FAGO, 98, 44. <https://www.persistent-identifier.nl/urn:nbn:nl:ui:25-f00fc883-07f8-4d9d-873e-e898d80750f1>
- Wong, C., Liew, J., Yusop, Z., Ismail, T., Venneker, R., & Uhlenbrook, S. (2016). Rainfall characteristics and regionalization in Peninsular Malaysia based on a high resolution gridded data set. *Water*, 8(11): 500. doi:<https://doi.org/10.3390/w8110500>
- Wu, W., Dandy, G. C., Maier, H. R., Maheepala, S., Marchi, A., & Mirza, F. (2017). Identification of optimal water supply portfolios for a major city. *Journal of water resources planning and management*, 143(9): 05017007.
- WWAP. (2019). The United Nations World Water Development Report 2019: Leaving No One Behind. Retrieved from <https://reliefweb.int/sites/reliefweb.int/files/resources/367306eng.pdf> f12/04/2020